Enhancement of Ethanol Vapor Sensing Properties of ZnO Nanoplates by Simple Composition with α-Fe_2O_3 Nanorods

Do Duc Tho[*], *Luong Huu Phuoc, Nguyen Duy Thanh, Nguyen Dinh Thieu, Vu Xuan Hien, Dang Duc Vuong, Nguyen Duc Chien*

Hanoi University of Science and Technology – No. 1, Dai Co Viet Str., Hai Ba Trung, Ha Noi, Viet Nam

Received: March 23, 2017; accepted: June 9, 2017

Abstract

ZnO nanoplates with average size of 200×400×40 nm and α-Fe_2O_3 nanorods with an average diameter and a length of 50 nm and several μm have been prepared through hydrothermal treatment method. Both materials were mixed in weight ratios (ZnO /α-Fe_2O_3) of 1/9, 2/8, 3/7, 1/1, 7/3, 8/2 and 9/1 to produce nanocomposite materials. Ethanol vapor properties of films derived from obtained materials, pristine nanoplates ZnO and pristine nanorods α-Fe_2O_3 were investigated at temperatures in the range of 300-400 °C and ethanol vapor concentrations in the range of 125-1500 ppm. The result shows that the material of 80 wt.% ZnO/ 20 wt.% α-Fe_2O_3 exhibits the highest response to ethanol vapor at 400 °C. The improvement in the ethanol vapor sensing characteristics of this material compared with pristine nanoplates ZnO and pristine nanorods α-Fe_2O_3 is attributed to the formation of heterojunctions in materials and their porous structure.

Keywords: ZnO nanoplates, α-Fe_2O_3 nanorods, ZnO/α-Fe_2O_3 nanocomposites, Ethanol vapor sensor

1. Introduction

ZnO is a traditional n-type semiconductor due to the existence of oxygen vacancies with wide, direct bandgap (3.37 eV, at 300K) and a large free exciton binding energy (60 meV). Its nanostructures have attracted intense research interest due to their morphologies and potential optical and electrical applications, such as field emitter [1], ultraviolet laser [2], biosensor [3], gas sensor [4-7] and UV devices [8-9].

Hematite (α-Fe_2O_3), an n-type semiconductor with a bandgap of 2.1 eV, is particularly attractive for gas-sensing applications due to its high chemical stability, low manufacturing cost, low toxicity and the most stable iron oxide under ambient environment. It is widely used in gas sensors, catalysts, high-density magnetic recording media, clinical therapy and diagnosis [10-14]. To date, a variety of α-Fe_2O_3 nanostructured materials in various geometrical morphologies have been successfully prepared, such as urchinlike [15], quasicubic [16], belts [17], tubes [18], nanorings [19], rods [20], hollow spheres [21], nano-rhombohedra [22].

Hetero-nanostructures consisting of two or more metal oxides have attracted increasing attention due to the possibilities of integrating the physical and chemical properties of these oxides. In the past year, coupled metal oxides were formed by ZnO and other metal oxides such as CuO, WO_3 for selective H_2S detection [23], H_2 gas sensing [24] and for photocatalytic degradation [25]. However, the composition of ZnO nanoplates and α-Fe_2O_3 nanorods for ethanol vapor sensing is rare. In this contribution, we prepared single crystalline ZnO nanoplates and α-Fe_2O_3 nanorods to produce ZnO/α- Fe_2O_3 nanocomposite materials by wet chemical method. The structures and their ethanol sensing properties of the composites also were studied.

2. Experimental

ZnO nanoplates and α-Fe_2O_3 nanorods were prepared by a wet chemical method according to Refs. [26] and [20]. The ZnO/α-Fe_2O_3 nanocomposite materials have been carried out by a simple mixing of the both components with different weight ratios. These obtained materials are presented in table 1.

Table 1. Prepared nanocomposite materials.

Sample name	ZnO (wt %)	α-Fe_2O_3 (wt %)
M1	10%	90%
M2	20%	80%
M3	30%	70%
M4	50%	50%
M5	70%	30%
M6	80%	20%
M7	90%	10%

[*] Corresponding author: Tel.: (+84) 162.898.7186
Email: tho.doduc@hust.edu.vn

Crystal structure identification of ZnO nanoplates and α-Fe_2O_3 nanorods were obtained using X'pert Pro (PANalytical) MPD and Burker-AXS (Siemens) D5005, respectively, with a CuKα radiation (λ = 1.54065 Å) at a scanning rate of 0.03°/2s in the 2θ range from 10° to 70°. The morphologies of nanopowder ZnO, α-Fe_2O_3 and composite of 30 wt.% ZnO/30 wt.% α-Fe_2O_3 (M3) were identified by a scanning electron microscope SEM (HITACHI S4800) using an electron beam energy of 10 kV.

3. Results and disscution

3.1. Material characteristics and morphologies

Characteristics of obtained pristine ZnO nanoplates and α-Fe_2O_3 were indicated elsewhere [26-27]. We observed that ZnO nanoplates have average size 200×400×40 nm. The peaks from XRD pattern can be indexed to the hexagonal wurtzite of ZnO with the lattice constant of $a = b = 0.3249$ nm and $c = 0.5206$ nm (JCPDS 36-1451). No detectable peak of impurities and other phases was observed, indicating the formation of single-phase. The diameter of obtained α-Fe_2O_3 nanorods was 50 nm. α-Fe_2O_3 has rhombohedral structure (JCPDS 33-0664) with lattice constant of $a = b = 0.5038$ nm, $c = 1,3722$ nm, $\alpha = \beta = 90°$, $\gamma = 120°$.

Fig.1a shows a SEM image of a nanocomposite of 70 wt.% ZnO /30 wt.% α-Fe_2O_3 (M5). The energy dispersive x-ray spectroscopy analysis (EDX) of M5 material is shown in Fig. 1b, which demonstrated that both elements Zn and Fe have been presented in material. There is no impurity element. The composition obtained from the EDX spectra is roughly consistent with the desired weight ratio of ZnO and α-Fe_2O_3.

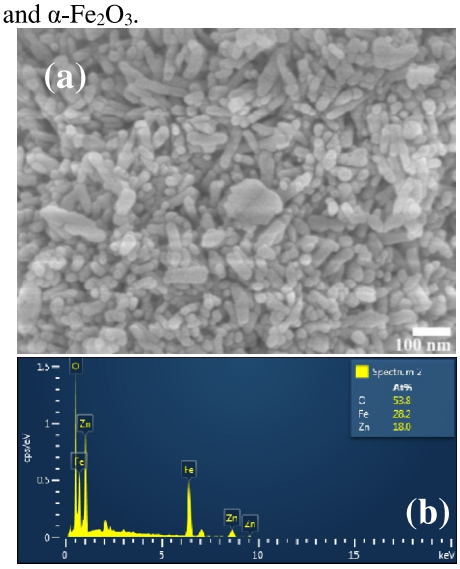

Fig. 1. SEM image (a) and EDX spectrum (b) of nanocomposite 70 %wt. ZnO/ 30 % α-Fe_2O_3 (M5).

3.2. Ethanol vapor sensing properties

These nanocomposite materials were coated onto Pt-interdigitated electrodes with gap of fingers 20 μm by spin-coating method to produce sensor samples. Afterward the all sensor samples were dried in air at 80 °C for 24h and heated at 600 °C for 2h to evaporate the organic species and to stabilize the materials structure. The sensor sample response is defined as a ratio, R_{air}/R_{gas}, where R_{air} is the resistances of sensor samples in dry air and R_{gas} is the resistances in different concentration of ethanol vapor. The response of these sensor samples to ethanol vapor was measured in static gas sensing system at temperatures in the range of 300-400 °C and ethanol vapor concentration levels of 125-1500 ppm.

Fig. 2 shows the response-recovery of the M6 sensor sample. We noted that the reference voltage increases with ethanol vapor concentration. It depicts that the material shows an n-type semiconductor property.

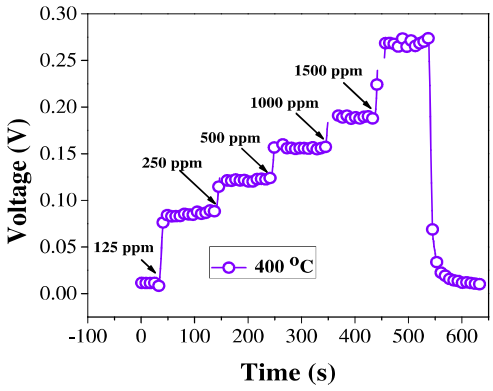

Fig. 2. Transient response of M6 sensor sample to ethanol vapor with concentration levels of 125-1500 ppm at 400 °C.

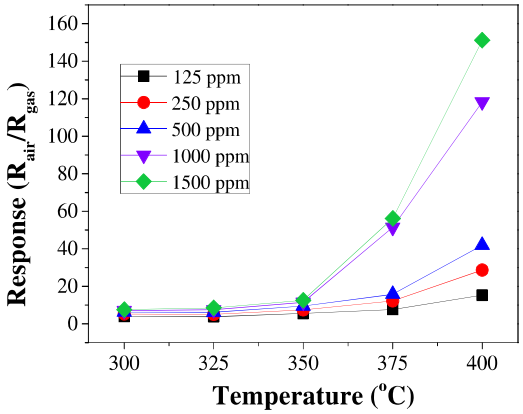

Fig. 3. The dependence of M6 sensor sample sensitivity to ethanol vapor on temperature.

Figure 3 shows the response of the M6 sensor sample as a function of temperature. As can be seen that its response reaches the largest value at 400 °C in the studied temperature range. Therefore, 400 °C was chosen as the testing temperature to investigate a dependence of the response to ethanol vapor concentration of other ZnO/α-Fe_2O_3 samples.

Figure 4 shows the responses of corresponding ZnO/α-Fe_2O_3, pristine α-Fe_2O_3 and pristine ZnO sensor samples when exposed to 1500 ppm ethanol vapor at 400 °C. At this temperature, the M6 sensor sample shows the highest response in comparing with other sensor samples including pristine α-Fe_2O_3 and pristine ZnO. Its response is 151 for 1500 ppm ethanol vapor. The result also indicated the sensitivity of the pristine ZnO materials to the ethanol vapor was improved by simple mixing ZnO with α-Fe_2O_3 in appropriate weight ratio and the best performance can be achieved with a composite of 80 wt.% ZnO/ /20 wt.% α-Fe_2O_3.

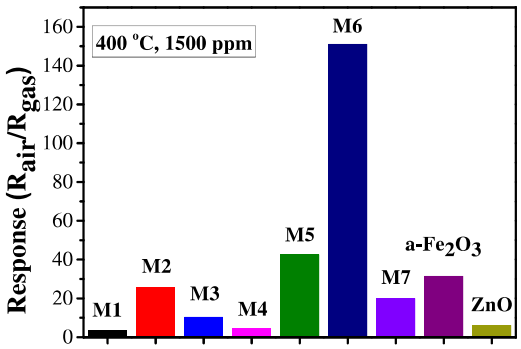

Fig. 4. The sensitivity of sensor samples to 1500 ppm ethanol vapor at 400 °C.

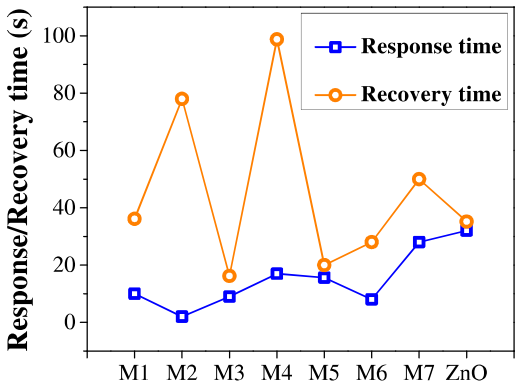

Fig. 5. Response time for 125 ppm and recovery time for 1500 ppm ethanol vapor at 400 °C of sensor samples.

In this case, the conduction and valence band of two oxides are discontinuous at the junction of two oxides due to their bandgap difference. It forms an additional potential barrier at the boundary between ZnO nanoplate and α-Fe_2O_3 nanorod which could influence on the response of the sensor sample.

When the ZnO/ α-Fe_2O_3 surfaces were exposed to ethanol vapor, the ethanol molecules diffuse through the metal oxide layer and the ZnO/ α-Fe_2O_3 interface, then penetrate in to the film. The ethanol molecules react with negatively charged oxygen ions located at ZnO/ α-Fe_2O_3 interface by reactions [28]:

$$C_2H_5OH+6O^- \rightarrow 2CO_2+3H_2O+6e^- \quad (1)$$

The time taken for the sensor sample to attain 90 % of maximum change in resistance on exposure to gas is the response time and the time taken by the sensor sample to get back 90% of the original resistance is the recovery time. Fig. 5 shows the response and recovery time of all sensor samples. They were calculated for 125 ppm and 1500 ppm ethanol vapor at 400 °C, respectively. It indicated that the response time of M6 sensor sample (8s) was little greater than one of sensor sample M2 (2s) but significantly smaller than one of other sensor samples and pristine ZnO (32s). Similarly, for 1500 ppm ethanol vapor the recovery time of M6 sensor sample (~28s) were significantly smaller than one of M1, M2, M4, M7 and pristine ZnO (~35s) sensor samples. Thus, in comparison with pristine ZnO nanoplates and α-Fe_2O_3 nanorods the appropriate composition of ZnO and α-Fe_2O_3 as M6 sensor sample not only enhances sensitivity but also reduces response/ response time.

4. Conclusion

In summary, we have presented a hydrothermal method for the synthesis of pristine ZnO nanoplates, α-Fe_2O_3 nanorods and their composites. The nanocomposite of 80 wt% ZnO /20 wt% α-Fe_2O_3 showed remarkably improved sensing properties for ethanol vapor compared to the pristine ZnO nanoplates, α-Fe_2O_3 nanorods and other composites at 400 °C. Its response to the 1500 ppm ethanol vapor is about 151. These results also show that the nanocomposite of 80 wt.% ZnO /20 wt.% α-Fe_2O_3 may be a promising material to fabricate ethanol sensor.

Acknowledgments

We are especially grateful to financial support of the project code T2016-PC-211.

References

[1] Y.W. Zhu, H.Z. Zhang, X.C. Sun, S.Q. Feng, J. Xu, Q. Zhao, B. Xiang, R.M. Wang, D.P. Yu, Efficient field emission from ZnO nanoneedle arrays, Applied Physics Letters. 83 (2003) 144-146.

[2] M.H. Huang, Room-Temperature Ultraviolet Nanowire Nanolasers, Science. 292 (2001) 1897-

1899.

[3] J.X. Wang, X.W. Sun, A. Wei, Y. Lei, X.P. Cai, C.M. Li, Z.L. Dong, Zinc oxide nanocomb biosensor for glucose detection, Applied Physics Letters. 88 (2006) 10-13.

[4] J.X. Wang, X.W. Sun, H. Huang, Y.C. Lee, O.K. Tan, M.B. Yu, G.Q. Lo, D.L. Kwong, A two-step hydrothermally grown ZnO microtube array for CO gas sensing, Applied Physics A: Materials Science and Processing. 88 (2007) 611-615.

[5] M. Hjiri, L. El Mir, S. Leonardi, N. Donato, G. Neri, CO and NO2 Selective Monitoring by ZnO-Based Sensors, Nanomaterials. 3 (2013) 357-369.

[6] C.-L. Hsu, K.-C. Chen, T.-Y. Tsai, T.-J. Hsueh, Fabrication of gas sensor based on p-type ZnO nanoparticles and n-type ZnO nanowires, Sensors and Actuators B: Chemical. 182 (2013) 190-196.

[7] Q. Wan, Q.H. Li, Y.J. Chen, T.H. Wang, X.L. He, J.P. Li, C.L. Lin, Fabrication and ethanol sensing characteristics of ZnO nanowire gas sensors, Applied Physics Letters. 84 (2004) 3654-3656.

[8] J.H. Jun, H. Seong, K. Cho, B.-M.M. Moon, S. Kim, Ultraviolet photodetectors based on ZnO nanoparticles, Ceramics International. 35 (2009) 2797-2801.

[9] L. Luo, Y. Zhang, S.S. Mao, L. Lin, Fabrication and characterization of ZnO nanowires based UV photodiodes, Sensors and Actuators, A: Physical. 127 (2006) 201-206.

[10] N.D. Cuong, D.Q. Khieu, T.T. Hoa, D.T. Quang, P.H. Viet, T.D. Lam, N.D. Hoa, N. Van Hieu, Facile synthesis of α-Fe_2O_3 nanoparticles for high-performance CO gas sensor, Materials Research Bulletin. 68 (2015) 302-307.

[11] H. Fan, T. Zhang, X. Xu, N. Lv, Sensors and Actuators B : Chemical Fabrication of N-type Fe_2O_3 and P-type $LaFeO_3$ nanobelts by electrospinning and determination of gas-sensing properties, Sensors & Actuators: B. Chemical. 153 (2011) 83-88.

[12] P.N. Hieu, P. Van Toan, N.P. Thang, D.D. Vuong, N.D. Chien, Synthesis and Gas-Sensing Properties of Hollow Sea Urchin-Like α-Fe_2O_3 Nanostructure, E-Journal of Surface Science and Nanotechnology. 9 (2011) 508-511.

[13] Y. V. Kaneti, Q.M.D. Zakaria, Z. Zhang, C. Chen, J. Yue, M. Liu, X. Jiang, A. Yu, Solvothermal synthesis of ZnO-decorated α-Fe_2O_3 nanorods with highly enhanced gas-sensing performance toward n-butanol, Journal of Materials Chemistry A. 2 (2014) 13283-13292.

[14] J. Bandara, U. Klehm, J. Kiwi, Raschig rings-Fe_2O_3 composite photocatalyst activate in the degradation of 4-chlorophenol and Orange II under daylight irradiation, Applied Catalysis B: Environmental. 76 (2007) 73-81.

[15] L.-P. Zhu, H.-M. Xiao, X.-M. Liu, S.-Y. Fu, Template-free synthesis and characterization of novel 3D urchin-like α-Fe_2O_3 superstructures, J. Mater. Chem. 16 (2006) 1794-1797.

[16] Y. Zheng, Y. Cheng, Y. Wang, F. Bao, L. Zhou, X. Wei, Y. Zhang, Q. Zheng, Quasicubic alpha-Fe_2O_3 nanoparticles with excellent catalytic performance., The Journal of Physical Chemistry. B. 110 (2006) 3093-3097.

[17] X. Wen, S. Wang, Y. Ding, Z. Lin Wang, S. Yang, Controlled growth of large-area, uniform, vertically aligned arrays of α-Fe_2O_3 nanobelts and nanowires, Journal of Physical Chemistry B. 109 (2005) 215-220.

[18] C.-J. Jia, L.-D. Sun, Z.-G. Yan, L.-P. You, F. Luo, X.-D. Han, Y.-C. Pang, Z. Zhang, C.-H. Yan, Single-Crystalline Iron Oxide Nanotubes, Angewandte Chemie International Edition. 44 (2005) 4328-4333.

[19] J.J. Chun, L. Feng, D.H. Xiao, T. George, R.L.S. Jorg, Large-Scale Synthesis of Single-Crystalline Iron Oxide Magnetic Nanorings, J. Am. Chem. Soc. 130 (2008) 16968.

[20] D.D. Vuong, K.Q. Trung, N.H. Hung, N. Van Hieu, N.D. Chien, Facile preparation of large-scale α-Fe_2O_3 nanorod/SnO_2 nanorod composites and their LPG-sensing properties, Journal of Alloys and Compounds. 599 (2014) 195-201.

[21] B. Mao, Z. Kang, E. Wang, C. Tian, Z. Zhang, C. Wang, Y. Song, M. Li, Template free fabrication of hollow hematite spheres via a one-pot polyoxometalate-assisted hydrolysis process, Journal of Solid State Chemistry. 180 (2007) 489-495.

[22] Z. Pu, M. Cao, J. Yang, K. Huang, C. Hu, Controlled synthesis and growth mechanism of hematite nanorhombohedra, nanorods and nanocubes, Nanotechnology. 17 (2006) 799-804.

[23] S.J. Kim, C.W. Na, I.S. Hwang, J.H. Lee, One-pot hydrothermal synthesis of CuO-ZnO composite hollow spheres for selective H_2S detection, Sensors and Actuators, B: Chemical. 168 (2012) 83-89.

[24] Y. Liu, J. Yu, P.T. Lai, Investigation of WO_3/ZnO thin-film heterojunction-based Schottky diodes for H_2 gas sensing, International Journal of Hydrogen Energy. 39 (2014) 10313-10319.

[25] S.M. Lam, J.C. Sin, A.Z. Abdullah, A.R. Mohamed, ZnO nanorods surface-decorated by WO_3 nanoparticles for photocatalytic degradation of endocrine disruptors under a compact fluorescent lamp, Ceramics International. 39 (2013) 2343-2352.

[26] D.D. Nguyen, D.T. Do, X.H. Vu, D.V. Dang, D.C. Nguyen, ZnO nanoplates surfaced-decorated by WO_3 nanorods for NH_3 gas sensing application, Advances in Natural Sciences: Nanoscience and Nanotechnology. 7 (2016) 15004.

[27] N.D. Dien, L.H. Phuoc, V.X. Hien, D.D. Vuong, N.D. Chien, Hydrothermal Synthesis and Ammonia Sensing Properties of WO_3/Fe_2O_3 Nanorod Composites, Journal of Electronic Materials. 46 (2017) 3309-3316.

[28] T. Gao, T.H. Wang, Synthesis and properties of multipod-shaped ZnO nanorods for gas-sensor applications, Applied Physics A: Materials Science and Processing. 80 (2005) 1451-1454.